Colloids and Surfaces B: Biointerfaces 241 (2024) 114038

Contents lists available at ScienceDirect

Colloids and Surfaces B: Biointerfaces

journal homepage: www.elsevier.com/locate/colsurfb

Self-assembling properties of mono and di-rhamnolipids characterized using small-angle X-ray scattering

Alessandra Marega Motta [a], Paolo Mariani [a], Rosangela Itri [b,*], Francesco Spinozzi [a,*]

[a] Department of Life and Environmental Sciences, Polytechnic University of Marche, Italy
[b] Applied Physics Department, Institute of Physics, University of São Paulo, São Paulo, Brazil

ARTICLE INFO

Keywords:
Small-angle x-ray scattering
Mono-rhamnolipid
Di-rhamnolipid
Biosurfactant
Volume fraction distribution
Chemical groups

ABSTRACT

Rhamnolipids are glycolipid surfactants composed by a hydrophilic head of either one (mono-RL) or two (di-RL) rhamnose moieties coupled to hydroxyaliphatic chains that can be of different lengths. In spite of their importance in different fields of applications, as bioremediation processes for instance, self-aggregation physicochemical properties of RLs are not unique. This because a variety of aggregates morphologies (shape and size) can either exist or coexist in aqueous dispersion due to mono-RL:di-RL molar ratio, hydrophobic tails length, pH and the presence of co-surfactants and additives. Recently, a theorethical approach reported the self-assembling morphologies of either pure mono or di-RL in aqueous environment, predicting the formation of spherical to ellipsoidal micelles to worm-like and disk-like aggregates depending on RL concentration and fatty acid chain length. In order to add new information to those previously available, the present work investigated the self-assembling properties of mono-RL-C10-C10 and di-RL-C10-C10 separately in aqueous dispersion by small angle X-Ray scattering (SAXS). A novel approach was applied to the data analysis coupling the scattering length density profiles of the RLs chemical groups and Monte Carlo simulations. Such an approach allowed us to infer about the preferred mono-RL and di-RL conformations that fit better in the self-assembling morphologies. In this way, we show that mono-RL-C10-C10 self-assembles into lamella-like aggregates coexisting with 30 % of multilamella aggregates (circa of 5 closed stacked lamella) from a concentration ranging from 10 to 50 mM, with hydrophobic thickness of about 12 Å, a hydrated polar head thickness of 10 Å, and an area per glycolipid of 76 $Å^2$. On the other hand, di-RL prefers to self-associate into flexible cylinder-like aggregates, from 70 mM to 110 mM concentration, with hydrophobic radius on the order of 7.5 Å, a hydrated polar shell of 21.5 Å, with hydropobic/polar interface of 110 $Å^2$ per glycolipid. Interestingly, the parameters obtained from the best fitting to the experimental data associated to the volume fraction distribution of the chemical groups within the aggregates revealed that the hydrophobic chains are more disordered in mono-RL planar aggregates than in di-RL worm-like aggregates, as well as the hydration properties. Further, the addition of 100 mM NaCl in di-RL aqueous dispersion leads to the formation of longer worm-like aggregates. Taking together, this work opens a new avenue regarding characterization of biosurfactants self-assembling properties by using SAXS, also contributing to prepare more efficient biosurfactant dispersions depending on the desired applications in industrial sectors and bioremediation.

1. Introduction

Rhamnolipids (RLs) are a class of biosurfactants produced by microorganisms widely studied due to their low concentration-surface tension activity at either air-liquid or liquid-liquid interfaces. Such characteristic allows applying RLs in different fields as the washing or cleaning industry, environmental remediation, cosmetic industry and pharmaceutical products [1–3]. Rhamnolipids are produced by *Pseudomonas aeruginosa* under appropriate conditions [4]. They are composed by two moieties: a hydrophobic lipid moiety with one or more saturated/unsaturated fatty acids chains, linked together with an ester bond, and a Rhamnose (RHA) moiety that is hydrophilic comprising mono or di (L)-rhamnose molecules linked through α-1,2-glycosidic linkage. They are known as mono and di-RL, respectively. Both moieties are linked via glycosidic linkage [5]. In particular, *P. aeruginosa* produces a heterogeneous mixture of mono and di-RLs with fatty acid tails

* Corresponding authors.
E-mail addresses: itri@if.usp.br (R. Itri), f.spinozzi@univpm.it (F. Spinozzi).

https://doi.org/10.1016/j.colsurfb.2024.114038
Received 7 March 2024; Received in revised form 31 May 2024; Accepted 12 June 2024
Available online 15 June 2024

of different lengths. The amphiphilic nature of RLs drives their interaction with biological membranes [6]. It has been previously shown that di-RL intercalates into the model membranes represented by phosphatidylcholine bilayers producing structural perturbations [7]. Further, it has been also shown that the mixture of di-RL and mono-RL has a DPPC bilayer disrupting effect which may be related with the haemolytic power of these molecules at high concentration [8]. More recently, our group purified mono-RL-C10-C10 and di-RL-C10-C10 and investigated each individual interaction with DOPC:Sphingomyelin:Cholesterol giant vesicles bilayers thus representing membranes containing Liquid-ordered (L_o) - Liquid disordered (L_d) phases coexistence (lipid-rafts) [9]. The results evidenced that while mono-RL (near and above the critical micellar concentration, cmc) increases lipid bilayer area without affecting membrane permeability, di-RL promotes L_o outward budding and pore formation in the L_d phase [9]. Certainly, such effects may be correlated with a cell membrane mysfunction under RLs interaction. It is then clear that mono-RL and di-RL can act differently on biological targets due to differences in their molecular structures. Therefore, it is of paramount importance to investigate not only the physicochemical properties of the RLs mixture, but also the ones of each component focusing on potential applications [10].

As highlighted in a recent review by Esposito et al. [3], despite numerous studies characterizing the aggregation and surface properties of RLs, there remains a lack of in-depth analysis regarding the morphology of micelle-like aggregates of these compounds in response to pH, salts, and RL compositions. Previous small-angle neutron scattering (SANS) data have reported aggregated shapes ranging from globular, cylinder-like micelles to small and large vesicles/lamellar structures, depending on factors such as pH value, mono-RL and di-RL molar ratio, fatty acid chain size, and the presence of additives and co-surfactants [11–14,15]. For example, SANS investigations at pH 9 [12] showed that mono-RL-C10-C10, at concentration below 20 mM, forms core-shell micelles that fully transform into unilamellar or bilamellar vesicles at concentration above 30 mM, whereas di-RL-C10-C10, in a concentration range from 20 to 100 mM, form only micellar structure. Recently, a dissipative particle dynamics method has been applied to investigate the self-assembly properties of mono and di-RL-C10-C10 and mono and di-RL-C16-C16 at concentrations varying from circa 17–150 mM [16]. The author obtained different mono and di-RL morphologies depending on the fatty acid tails and biosurfactant concentration ranging from spherical and ellipsoidal vesicles to worm-like and disc-like micelles. More recently, Baccile et al. [17] performed an extensive study, based on small angle X-ray scasttering (SAXS) and cryogenic transmission electron microscopy (cryo-TEM), on the properties of mono-RL-C10-C10 and di-RL-C10-C10, together with mono-RL-C10 and C10-C10, by varying biosurfactant concentration and pH. Their results confirmed that di-RL-C10-C10, in a wide range of pH, form micelles (described with a core-shell ellipsoid with uneven shell thickness), whereas mono-RL-C10-C10, on going from basic pH to acidic pH undergoes a transition, centered at pH = 6.5, from micelles to vesicles, these latter modeled as flat bilayers. To note, in all cases experimental SAXS curves showed a power-law behaviour at scattering angle, suggesting the presence of large aggregates. In order to contribute to this field and to experimentally verify the self-assembling properties of mono-RL-C10-C10 and di-RL-C10-C10 separately, the present work is undertaken. To do so, synchrotron SAXS experiments were carried out from mono-RL-C10-C10 and di-RL-C10-C10 aqueous samples at pH 7.5 for concentrations varying from 10 mM to 110 mM, respectively, well above the cmc values (0.093 mM for mono-RL and 0.054 mM for di-RL [9]). In the case of di-RL, salt samples containing 100 mM NaCl were also investigated due to the interest on the use of RLs in marine bioremediation process. Of note, mono-RL precipitated in the presence of NaCl. Herein, we analysed the SAXS data through a novel methodology based on electron density profiles associated to a combination of the volume fraction distributions of the main chemical groups constituting the mono-RL and di-RL molecules, respectively. Such chemical group approach allowed us properly considering the structure of the biosurfactant molecule that self-assembles in a micelle-like aggregate of a preferred morphology (shape and size). A simple Monte Carlo analysis of the chemical volume distributions has been further developed which permitted us to infer the most preferred RLs conformations inside each micellar aggregate.

2. Materials and methods

2.1. Rhamnolipids separation

Rhamnolipids from *P. aeruginosa* (in powder and purity of 90 %) was purchased from Sigma-Aldrich (Poole, UK). The separation of mono-RL and di-RL from the rhamnolipids mixture was carried out using column chromatography as described by Sánchez et al. [18]. Briefly, silicagel 60 in chloroform (Sigma-Aldrich, purity > 99 %) was packed into a glass chromatography column (2 × 40 cm). Subsequently, 2.0 g of the crude rhamnolipid mixture was dissolved in 4 mL of chloroform and loaded into the column. The column was washed with chloroform until neutral lipids were completely eluted, followed by chloroform/methanol solutions at 50:3 and 50:5 ratios, which extracted the mono-rhamnolipid component, and chloroform/methanol solutions at 50:50 ratios and pure methanol, which extracted the di-rhamnolipid component. The chemical characterization of the compounds was confirmed by electrospray mass spectroscopy [5]: the sample containing mono-RL was mainly composed of molecules with molecular weight of 502 Da, whereas most of the molecules in the di-RL sample showed a molecular weight of 648 Da. According to the literature, these molecular weights are attributed to the structural formulas of mono-RL and di-RL, respectively [5].

2.2. SAXS samples preparation for mono-RL and di-RL and performed experiments

We have investigated, using SAXS technique, solutions of either mono-RL or di-RL obtained by means of the chromatographic separation, as discussed above. Samples were dispersed in milliQ water at different concentrations well above the cmc, from 10 to 100 mM and, for di-RL, in the presence of NaCl. In detail, di-RL samples in pure water have been prepared at concentrations of 70, 90 and 110 mM (thus varying from 1296 × cmc to 2037 × cmc) and di-RL samples in the presence of 100 mM NaCl have been prepared at the concentrations 75, 80, 85, 90 and 110 mM. Regarding mono-RL, samples in pure water have been prepared at concentrations of 10, 18, 34 and 50 mM (thus varying from 107 × cmc to 547 × cmc); no measurements were carried out in the presence of NaCl since this salt causes the total precipitation of mono-RL. The pH of all the investigated samples was 7.5 ± 0.1. We have carried out a campaign of SAXS/WAXS (Wide-Angle X-ray Scattering) measurements at the beam-line I22 of the synchrotron Diamond (Didcot, UK) [19]. Due to the covid-19 pandemics, samples have been sent to the synchrotron Diamond by exploiting the mail-in program. After shipment, the samples remained completely intact, with no presence of precipitates. The same integrity conditions were also verified after the SAXS measurements. I22 was used in transmission mode and the dilute solutions of either mono-RL or di-RL were placed in polycarbonate capillaries. The camera length was 3.0 m and the related range of q was comprised between 0.008 and 3.23 $Å^{-1}$. All measurements were obtained at 20° C. SAXS patterns were recorded with a Pilatus P3–2 M detector operating with 1475 × 1679 pixels, each with 172 × 172 μm^2 size. WAXS signals were collected by a Pilatus P3–2 M-DLS-L detector working with the same number and size of pixels. SAXS and WAXS raw data have been preliminary treated with the software Dawn operating at I22, in order to obtain the radial averages for both SAXS and WAXS curves. Subsequently, we have processed all the curves by a home-made software written under Gnuplot [20], aimed to perform a proper empty capillary subtraction, and followed by a buffer subtraction. SAXS and

WAXS profiles, these latter up to 0.8 $Å^{-1}$ (before the broad diffraction band of water), have been merged in a unique SAXS curve by optimizing their overlap in a common q range. Absolute scale calibration has been calculated considering the scattering of pure water.

2.3. SAXS analysis for mono-RL and di-RL-containing solutions

All SAXS curves have been analyzed in the whole range of the scattering vector modulus, ($q = 4\pi\sin\theta/\lambda$, 2θ being the scattering angle and $\lambda = 1$ Å the X-ray wavelength) by using the Genfit software [21]. Different models were adopted, all available in the Genfit platform, and their reliability was evaluated not only by considering the reduced chi-square but also the physical adequacy of the optimized parameters. At the end of this fitting strategy, the most suitable model to interpret mono-RL SAXS data was that of planar bilayers with very large lateral dimensions and lamellar interactions. Regarding the di-RL SAXS data, the most suitable model was that of flexible cylindrical (worm-like) micelles spatially organized according to a fractal distribution. For both models, the electron density profile was described as a combination of the volume fraction distributions of the main chemical groups constituting the mono-RL and di-RL molecules, respectively. For mono-RL, the so-called modified scattering density profile (MSDP) model, described in detail by De Rosa et al. [22] and working in planar geometry, was adopted. For the di-RL case, the same chemical group approach but operating in cylindrical coordinates and described by Yoneda et al. [23], was exploited. To note, in both geometries, the volume fraction distribution function of each group is expressed by a combination of error functions. The advantage of the chemical group approach, compared to more traditional approaches, in which SAXS data are analyzed only in terms of thicknesses and electron densities, is the possibility to properly consider the structure of the surfactant molecule, thus avoiding to give credit to solutions which, despite are leading to a good fit of the data, do not agree with the composition of the sample. In the next sections, we summarize the main features to the two models.

2.4. SAXS model of mono-RL

The macroscopic differential scattering cross section (shortly referred to as the scattering intensity) of randomly oriented and partially interacting planar bilayers is given by

$$\frac{d\Sigma}{d\Omega}(q) = \frac{c_V}{D_B} r_e^2 \frac{2\pi}{q^2} A_z^2(q)\left[1 + x_{\mathrm{corr}}\left(S_{PT}^{N_c}(q) - 1\right)\right]. \quad (1)$$

In this equation, c_V is the dry surfactant volume fraction, D_B is the so-called Luzzati length, corresponding to the thickness of the dry lipid bilayer, r_e is the classical radius of the electron ($0.28179 \cdot 10^{-12}$ cm) and x_{corr} is the fraction of bilayers that form lamellar stacks. The two functions that depend on the modulus of the scattering vector, q, are $A_z(q)$, the Fourier transform of the excess electron density profile, $\rho(z) - \rho_0$, along the direction z perpendicular to the bilayer (ρ_0 being the solvent electron density) and $S_{PT}^{N_c}(q)$, the structure factor of stacked bilayers, here described by the para-crystal (PT) theory [24–27–30]. In the MSDP model, the electron density profile is written as a linear combination of the volume fraction distribution, $\varphi_i(z)$, of all the N chemical groups (including hydration water) that form the surfactant molecule, $\rho(z) =$

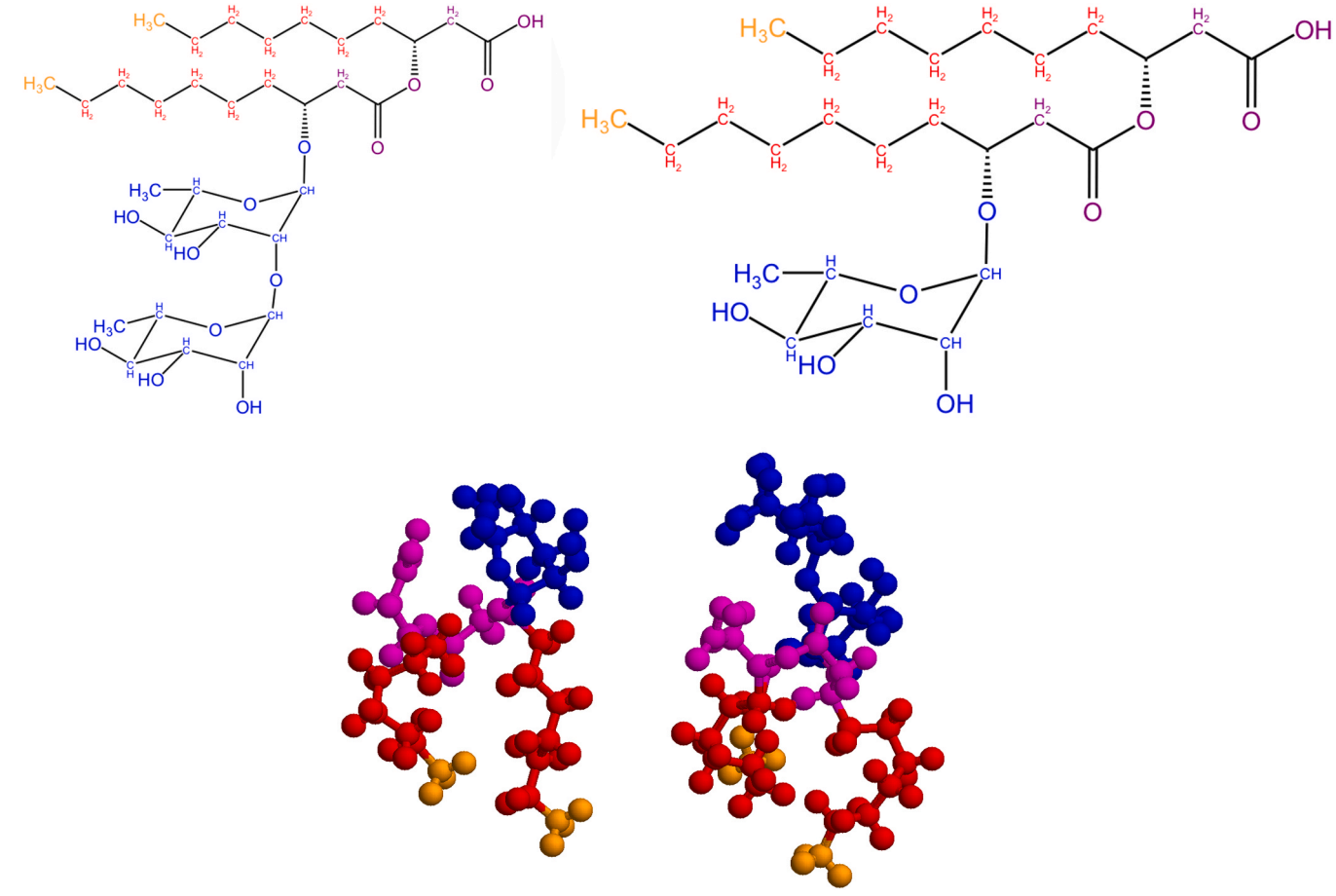

Fig. 1. Structure (top) and ball-and-stick representation (bottom) of mono-RL (left) and di-RL (right). Red, orange, magenta, and blue, correspond to CH_2, CH_3, the negatively group CR ($(CH)(CH_2)(COO)(CH)(CH_2)(COO^-)$), the rhamnose group RHA ($O(CHO)(CHCH_3)(CHOH)_3$) or the rhamnose-rhamnose group RHA-RHA ($[O(CHO)(CHCH_3)(CHOH)_2(CH)]_2(OH)$).

$\sum_{i=1}^{N}\rho_i\varphi_i(z)$, where $\rho_i = e_i/\nu_i$ is the electron density of the i-group, corresponding to the ratio between the number of electrons contained in the group (e_i) and the group volume (ν_i). Fig. 1 presents the chemical groups of mono-RL molecule here considered. Since bilayers are considered totally symmetric, the functions $\varphi_i(z)$ are symmetrical in respect to the bilayer center ($z = 0$) and, according to the MSDP approach, they are defined by the position z_i of the peak, corresponding to the coordinate where the volume fraction distribution of the i-group shows a maximum, the peak width $2w_i$ and the peak smoothness σ_i (the standard deviation of the error function). To note, by definition, the volume fraction distributions, for any z, should respect the constraint $\sum_{i=1}^{N}\varphi_i(z) = 1$. Moreover, they are related to both the area per surfactant molecule, a, and the chemical composition of the surfactant by the equation $\int_0^\infty \varphi_i(z)dz = n_i\nu_i/a$, where n_i is the number of i-chemical groups of the surfactant. The dominant hydrophobic group (typically CH_2, labeled with $i = 1$) and the hydration water molecules (group with $i = N$) are treated differently from all the other groups in order to ensure that they occupy all the available volume in the hydrophobic and in the polar domains of the surfactant, respectively. It is worth commenting that the dry volume fraction of mono-RLs is related to their molar concentration, C_m, by $c_V = C_m N_A \sum_{i=1}^{N-1}\nu_i$, where N_A is Avogadro's number. The parameters of the structure factors are the average bilayer distance, c, the number of correlated bilayer, N_c, and the so-called distortion factor, g_c, which is the ratio between the standard deviation σ_c of the Gaussian describing the staking disorder and the average distance c.

2.5. SAXS model of di-RL

The SAXS curves of di-RL have been successfully analyzed by modeling flexible and cylindrically shaped micelles with possible fractal interactions between them,

$$\frac{d\Sigma}{d\Omega}(q) = CN_A r_e^2 P_{wl}(q)A_r^2(q)S_M(q), \tag{2}$$

where C is the molar concentration of such worm-like particles. Here, $P_{wl}(q)$ is the form factor of thin chains according to the Pedersen-Schurtenberger [31] model, where the chains are seen as sequences of n_b statistical segments of length b (Khun length). The function $A_r(q)$ is the Fourier transform of the excess electron density profile in the radial direction r perpendicular to each chain segment, depicted by the equation $\rho(r) = \sum_{i=1}^{N}\varphi_i(r)$, where $\varphi_i(r)$ accounts for the radial volume fraction distribution of the i-chemical group (Fig. 1), with the constraint $\sum_{i=1}^{N}\varphi_i(r) = 1$. The functions $\varphi_i(r)$ are modeled by a combination of error functions, hence they are defined in terms of the radial position of the peak, r_i, the peak width $2w_i$ and the peak smoothness σ_i. However, in the radial geometry, these functions should respect the integral property $2\pi\int_0^\infty \varphi_i(r)dr = \overline{n}_a n_i \nu_i$, where $\overline{n}_a$ is the ratio between the number of surfactant molecules contained in the cylinder associated to each segment of the chain and b. A detailed explanation of the method is reported in the Sections S1-S4 of Supplementary Material (SM). Notice that, according to this model, the hydrophobic radius, R_{hyd}, the radius of the dry cylinder, R_B, conceptually similar to the Luzzati length of a bilayer as well as the overall radius of the cylinder, R, which include the hydration water molecules around the polar heads can be determined (see Eqs. S17-S19 of SM) as a function of the set of N radial volume fraction distributions $\varphi_i(r)$. The area per molecule at the hydrophobic polar-head interface and at the polar-head water interface are $a_{hyd} = 2\pi R_{hyd}/\overline{n}_a$ and $a = 2\pi R_B/\overline{n}_a$, respectively. The overall aggregation number of surfactant molecules in the worm-like micelle is $N_{agg} = \overline{n}_a n_b b$, hence the molar concentration of worm-like particles reads $C = C_d/N_{agg}$, where C_d is the molar concentration of di-RL molecules. The term $S_M(q)$ in Eq. 2 is the so-called measured structure factor, which takes into account the possible correlation between rigid segments belonging of different worm-like chains, according to $S_M(q) = 1 + \beta(q)[S(q) - 1]$, where $\beta(q)$ is the coupling function defined in terms of the geometry of the rigid segment (see Eq. S64 in SM) and is the structure factor here described by the Teixeira fractal model (see Eq. S63 in SM). Parameters of this model are the radius of the inhomogeneities, r_0, the fractal dimension, d_f, and the average correlation distance ξ between two inhomogeneities.

2.6. Global fit of SAXS data

The list of mono-RL's and di-RL's chemical groups and their physical-chemical features are shown in Table S1 of the SM. There are two hydrophobic groups, CH_2 and CH_3, and four polar groups, CR, RHA or RHA-RHA for either mono-RL or di-RL (Fig. 1), Na^+ and H_2O. Notice that, since for both surfactants the lyophilisation pH was 7.5, the carboxyl group in CR is almost fully dissociated so that there is nominally one sodium counter ion for each of the two molecules. However, the fraction of Na^+ that effectively remains within the polar head in the water dispersions of mono-RL and di-RL, α_{Na}, is considered a fitting parameter. In order to derive in an efficient manner the model parameters, it is preferable to fit with a unique calculation a set of SAXS curves measured for the same kind of sample and for some chemical-physical conditions. In this way it is possible to define parameters that are common to all the curves (common fitting parameters) and other fitting parameters that belong to a single curve (single-curve parameters). In our models, we have selected as common parameters only the volume of the methylene group, ν_{CH_2}, the ratio between the volume of the methyl group and the one of the methylene groups, r_{13}, and the volumes of the three polar groups, ν_{CR}, ν_{RHA} and $\nu_{RHA\text{-}RHA}$. All the other parameters have been considered single-curve parameters. However, in order to increase the robustness of SAXS data analysis and to avoid unlikely oscillations of structural as well as scattering parameters when the physical-chemical conditions of two samples are very close, we have exploited a regularization algorithm [32–34]. On this framework, the ensemble of SAXS curves, recorded for either mono-RL or di-RL samples, has been simultaneously analyzed performing the minimization of the score function $H = \chi^2 + \alpha\Psi$, where χ^2 is the classical reduced chi square of the set of N_m SAXS curves,

$$\chi^2 = \frac{1}{N_m}\sum_{m=1}^{N_m}\sum_{i=1}^{N_{q,m}}\frac{1}{N_{q,m}}\left(\frac{\frac{d\Sigma}{d\Omega_{m,ex}}(q_i) - \frac{d\Sigma}{d\Omega_{m,th}}(q_i)}{\sigma_m(q_i)}\right)^2 \tag{3}$$

$N_{q,m}$ being the number of points of the m-experimental scattering curve, $\frac{d\Sigma}{d\Omega_{m,ex}}(q_i)$, with experimental uncertainty $\sigma_m(q_i)$, that should be fitted by the theoretical SAXS curve $\frac{d\Sigma}{d\Omega_{m,th}}(q_i)$. Ψ represents the regularization factor

$$\Psi = \sum_{i=1}^{N_s}\sum_{m=1}^{N_m}\left(1 - \frac{X_{i,m'}}{X_{i,m}}\right)^2, \tag{4}$$

where $X_{i,m}$ is the i-th, among N_s, single-curve fitting parameters used to fit the m-th curve and $X_{i,m'}$ the parameter of the same kind used to fit the m'-th curve. This m'-th curve is that of the sample which has the chemical-physical characteristics (RL concentration or NaCl concentration, see the next Sections) most similar to those of the sample of the m-th curve. The constant α is selected in such a way that near the end of the minimization, when $\chi^2 \approx 1$, the product $\alpha\Psi$ is 10–20 % of χ^2. By repeating several times (typically 50 times) the minimization of H, the standard deviations of all fitting parameters can be estimated.

3. Results and Discussion

3.1. SAXS from mono-RL aqueous solutions

Log-log plots of the SAXS curves recorded at Diamond (I22 beamline) from mono-RL samples are shown in Fig. 2, panel A. To note, at low q, corresponding to the region of the 2D detector closer to the beam-stop (a region that will be described by a small number of pixels - some of them have indeed been masked in order to avoid considering spurious reflections) the points are affected by a higher error bar.

We first observe that at low q the behavior of the curves does not follow a q^{-2} trend, typical of infinite or large bilayer or a q^{-4} trend, characteristic of large aggregates. Conversely, such a trend is observed in the SAXS data recently published by Baccile et al. [17] for mono-RL-C10-C10 and di-RL-C10-C10 samples at pH close to 7.5. This notable difference can only be attributed to a difference in the purification procedure of our samples compared to that followed by Baccile et al. [17]. Moreover, at intermediate $q \sim 0.2$ Å^{-1}, a quite broad peak is clearly present, with a profile different from that typical of a bilayer band. On the basis of these observations, and after having attempted to analyze the data with different types of micellar aggregates, we evaluated that the model more suited to analyze these SAXS curves was that of a mixture of vertically correlated and uncorrelated bilayers, as discussed in Section 2.4. The global-fit analysis, which includes the regularization method, of all mono-RL SAXS curves has led to the best fitting curves shown as solid black and white lines in Fig. 2A. Final values of the merit function H, the reduced chi squared χ^2 and the regularization term $\alpha\Psi$, obtained with $\alpha = 10^{-1}$, are 1.09, 1.05 and 0.04, respectively. The common fitting parameters, together with their validity ranges, are shown in the first part of Table S2 of the SM. It is worth noticing that the volume of rhamnose (200.7 ± 0.8 Å^3) is close to the one predicted by the ACD/Labs Percepta Platform [35]. The single curve fitting parameters are shown as a function of mono-RL concentration in Figure S1 of the SM.

Considering their uncertainties, it is evident that they are almost independent of the biosurfactant concentration. Their average values, including their standard deviations as well as their adopted validity ranges, are reported in the central part of Table S2 of the SM. Other parameters derived from the fitting parameters are reported in the bottom part of Table S2 of the SM. The area per polar head (76.5 ± 0.4 Å^2) is in agreement with a structural organization of two-chain amphiphilic molecules in flat bilayers [36–38]. The fraction of sodium counter ions close to the polar heads is approximately 40 %, a result that should be evaluated considering that there are 25.0 ± 0.3 water molecules per polar head, with a mass density relative to bulk water of 0.966 ± 0.009. The trends of the volume fractions of the chemical groups, shown in Fig. 2B, show a markedly enlarged distribution of both the methyl group (orange curve) and the methylene groups (red curve), suggesting a high disorder of the two hydrophobic chains. The two polar groups, CR and RHA (magenta and blue curves, respectively), have partly overlapping distributions, indicating a partial side-by-side position of them with respect to the vertical axis of the bilayer. Finally, the peculiar distribution of water (green curve), slightly overlapped with the ones of hydrophobic groups, further confirms the high degree of chains' disorder. The fraction of vertically correlated bilayers is ≈ 30 %, with a repetition distance $c = 33.1 \pm 0.3$ Å (Table S2 of the SM), a distortion factor of approximately 0.12 and a small correlation number of ≈ 5. To note, c is comprised between t and $2D$, the former being the bilayer thickness calculated only considering position and wideness parameters, the latter including also the smoothness parameters. This result indicates that few correlated bilayers are almost in contact. A final note deserves the short thickness of the hydrophobic domain, $D_{hyd} = 5.80 \pm 0.02$ Å, corresponding at the z coordinate where $\varphi_{CH_2}(z) = 0.5$ (Fig. 2B): it can be further deduced that the two short chains of 7 carbon atoms are rather distributed in the lateral direction in order to cover, on average, the area of about 76 Å^2 (Table S2 of the SM). Fig. 2C presents the correspondent electron density profiles from each group in the planar bilayer (colored lines) as well as the total electron density profile (dark line). Of note, such a profile points to the fact that the total electron density can be well represented by two levels of distinct electron densities in respect to the electron density of the aqueous solution around 0.33 e/Å^3, thus representing the polar and apolar environments, as usually considered to analyse SAXS data of lamella-like micelle aggregates. In this scenary, the maximum electron density is around 0.4 e/Å^3 at circa 10 Å from the center of the bilayer, whereas the mininum electron density is centered in the middle of the bilayer with value of 0.26 e/Å^3.

To give a step forward in the data representation, a Monte Carlo (MC) method has been developed with the aim of correlating the volume fraction distributions of the chemical groups extracted from the SAXS curves (Fig. 2B) to the mono-RL possible conformations that take place inside the bilayer model, as described in Section S5 of SM. Accordingly,

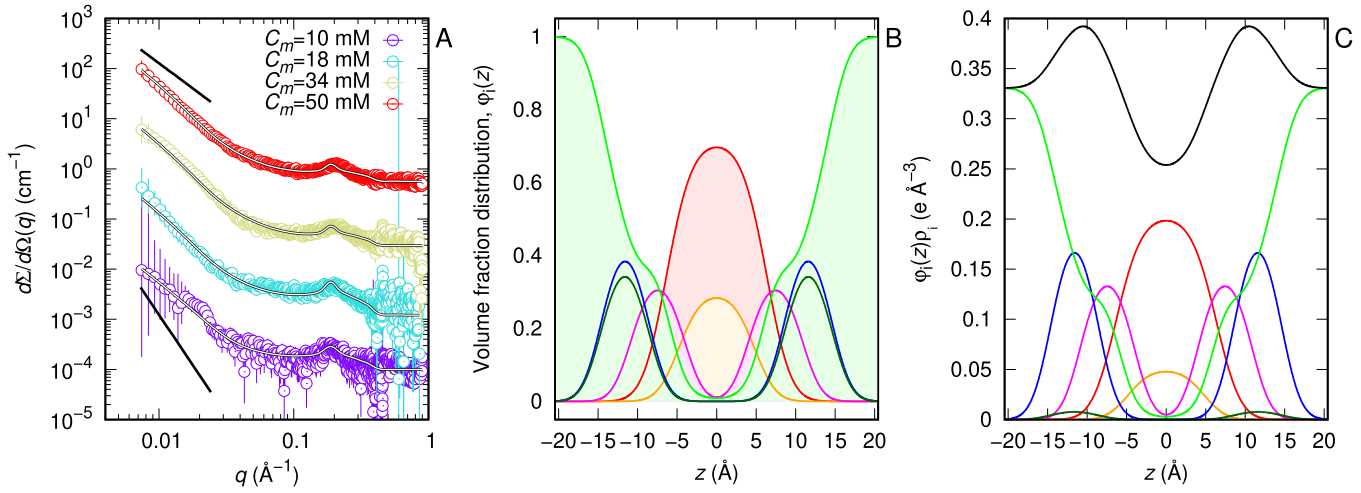

Fig. 2. A) Log-log plot of SAXS curves from mono-RL samples and their best fits obtained with the MSDP model. Curves have been stacked by a factor 10^k, where k is the index of the curves, starting from the one at the bottom with $k = 0$. The short straight lines on the top and on the bottom represent a q^{-2} and a q^{-4} trend, respectively. B) Volume fraction distribution of the chemical groups of mono-RL resulting from the fit of the curve at $C_m = 50$ mM. Red, orange, magenta, blue, dark-green and green lines correspond to CH_2, CH_3, CR, RHA (the reader must referred to Fig. 1), Na^+ and H_2O groups. The curve of Na^+ has been multiplied by a factor 100 for clarity. C) Electron density profile (black line) calculated from the volume fraction distributions shown in panel B along with the contribution of each chemical group (colored lines).

in the bilayer geometry (planar model) a set of mono-RL conformations gives rise to the volume fraction distributions through Eq. S74 which best fit the volume fraction distributions obtained from SAXS. As an example, Fig. 3A presents the 20 most representative mono-RL conformers obtained by the best MC method fitting to the volume fraction distributions retrieved from the SAXS curve of 50 mM mono-RL aqueous solution in the absence of salt (Figures S3 and S4), whereas Fig. 3B represents the corresponding bilayer formed by the organization of these conformers according to the best fit parameters described on Table S2 of the SM.

It should be remarked that a previous work [16] investigated the influence of the chemical structure of RLs on their self-assembly morphology. Simulations of four rhamnolipid congeners at surfactant concentrations ranging from 20 to 180 mM were considered. In particular, the result for mono-RL-C10-C10 predicted that at concentration of 20 mM irregularly shaped aggregates are formed. It was observed that the hydrophilic beads are packed inside the hydrophobic beads, showing a tendency of vesicular formation. As the concentration increases (for 70 mM, for instance) the enclosed water space expanded into a vesicle-like aggregate for higher mono-RL concentrations. Here, we experimentally show that mono-RL-C10-C10 self-assembles into planar bilayers of same dimensions, independent of the concentrations from 10 mM to 50 mM.

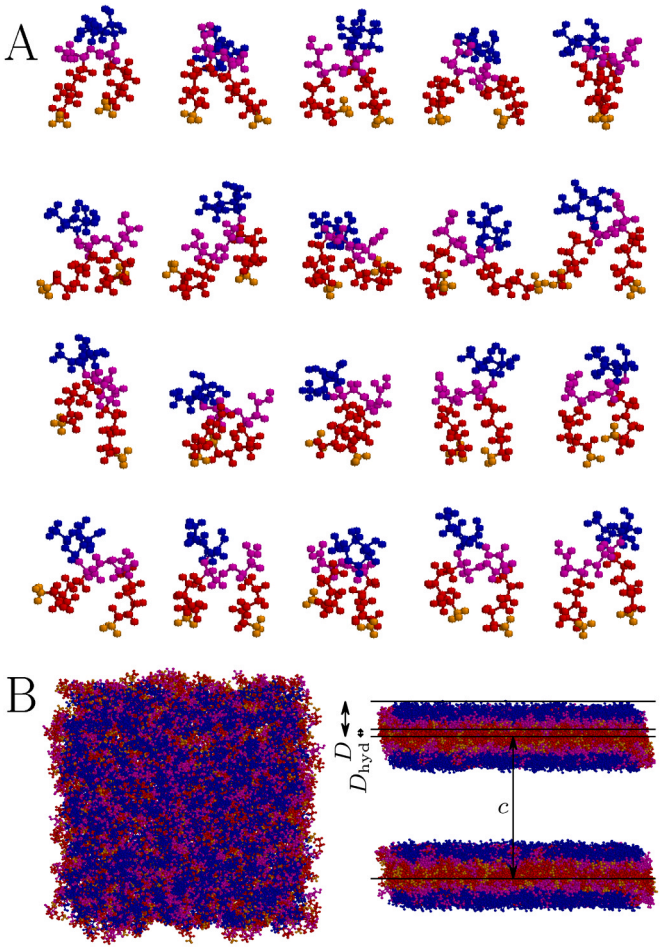

Fig. 3. A) The 20 most preferred mono-RL structural conformations within the planar bilayer model, calculated by the Monte Carlo method (Eq. S74), which best associate to the volume fraction distributions derived from the analysis of the SAXS curve with C_m = 50 mM and [NaCl]=0 mM (Figures S3 and S4). B) Representation of a mono-RL planar bilayer obtained with the best 20 conformers shown on panel A. Vertical double arrows indicate the hydrated monolayer thickness, D, the thickness of the hydrophobic monolayer domain, D_{hyd}, and the average bilayer distance, c, respectively.

3.2. SAXS from di-RL aqueous solutions

SAXS curves of di-RL samples, recorded at the I22 beamline of Diamond at 0 and 100 mM NaCl, are shown in Fig. 4A and 5A, respectively. To note, the WAXS branches are easily identifiable at high q, as they show a lower standard deviation.

Results clearly show that the presence of 100 mM NaCl (Fig. 5A) mainly modifies the low q region, which show a positive deviation with respect to the flat behavior, as seen for the curves in the absence of NaCl (Fig. 4A), which is typical of weakly interacting particles. We also stress that, at low q values, none of the curves displays a $q^{-\alpha}$ trend, as observed in the SAXS data published by Baccile et al. [17]. This further confirms the distinction, attributable to differences in the purification procedure, between our samples and those of Baccile et al. [17]. The solid black and white lines in Figs. 4A and 5A represent the best fits that we have obtained with the flexible and cylindrically shaped micelles model, introduced in Section 2.5. All curves have been fitted by a unique calculation, with the regularization method introduced above and separately applied to the two sets of SAXS curves at 0 and at 100 mM NaCl, respectively. Final values of the merit function H, the reduced chi squared χ^2 and the regularization term $\alpha\Psi$, obtained with $\alpha = 10^{-1}$, are 0.92, 0.83 and 0.09, respectively. In Table S3 of the SM, the model parameters (distinguished in three groups, common parameters, average of single-curve parameters and average of derived parameters - these two groups separately calculated for 0 and 100 mM NaCl) are reported, together with their validity ranges.

The volume of the methylene group, 26.42 ± 0.08 Å^3, is approximately 6 % lower than the one obtained for mono-RL, suggesting a lower disorder degree of the chains. On the contrary, ν_{CR} does not change from mono-RL to di-RL case. We note that the volume of the di-rhamnose group, which differs by one OH group in respect to two rhamnose groups, is 362 ± 4 Å^3. Regarding the single-curve fitting parameters, we notice that the ones related to the hydrophobic groups ($\overline{n}_a$, σ_{CH_2}, w_{CH_3}, and σ_{CH_3}) do not change with the amount of NaCl. Hence the radius of the hydrophobic domain, R_{hyd}, remains as large as approximately 7.5 Å, a value that exceeds of 2.5 Å the one obtained for the mono-RL case in planar geometry, confirming the lower degree of chains' disorder. The polar groups' parameters are slightly more sensitive to the presence of NaCl: in particular, the fraction of sodium counterions increases from ≈ 0.3–1.0 on going from 0 to 100 mM NaCl, as expected. The Luzzati-like radius, R_B, is ≈ 11.4 Å for the two set of samples, whereas the radius calculated from the model error functions parameters, R, is much larger and amounted to 29 Å at 0 mM NaCl and 36 Å at 100 mM NaCl. As a consequence, being in cylindrical geometry, the surfactant area at the hydrophobic - polar interface is ≈ 110 Å^2, whereas the one at the polar - bulk water interface is much larger, corresponding to ≈ 450 ^{2} so that there is space to accommodate approximately 200 hydration water molecules. All these features regarding the form factor can be better appreciated by observing the volume fraction distributions reported as a function of the radial distance in Figs. 4B and 5B. The methyl distribution (orange curves) show a more marked peak than the one of the mono-RL shown in Fig. 2B, whereas the blue trends representing the RHA-RHA volume fraction distribution spans a large distance when compared with the analogous of the RHA group for mono-RL. To note, the large green band attributed to the hydration water molecules. The effect of NaCl can be evaluated by comparing the dark-green curves (both multiplied by a factor 100 for clarity) in Figs. 4B and 5B: this latter is not only, on average, more intense, due to the higher values of α_{Na} at 100 mM NaCl, but its maximum is slightly shifted toward the CR group, indicating an higher penetration of the sodium cation in the polar head. Similar differences can also be observed in Figs. 4C and 5C, where the radial electron density profiles of each group (illustrated by colored lines) as well as the total electron density profile (represented by the dark line) are plotted. It is noteworthy that, compared to the electron

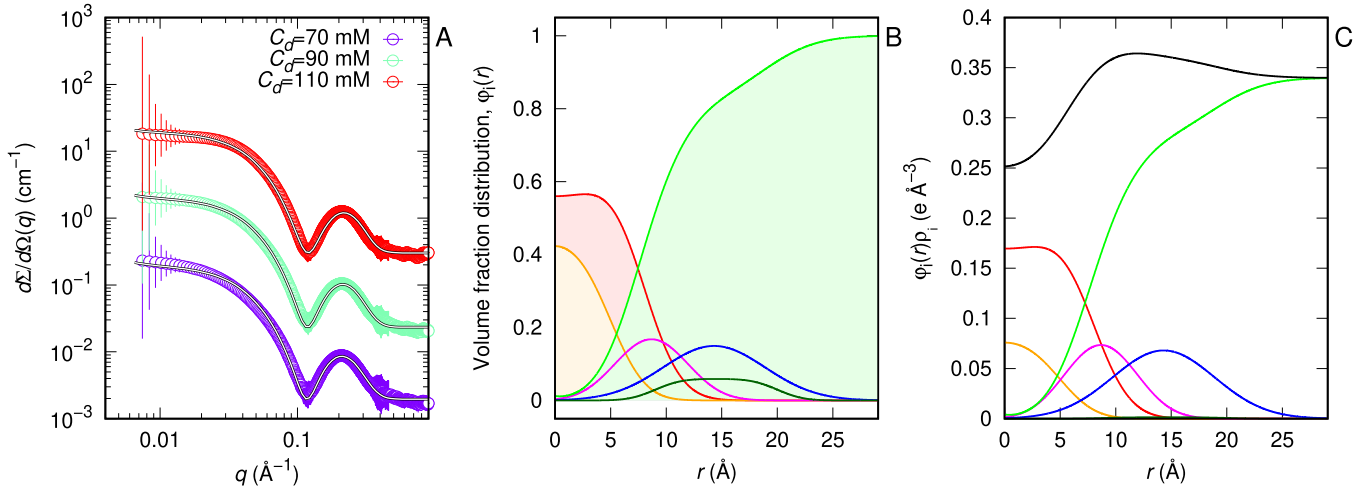

Fig. 4. A) Log-log plot of SAXS curves of di-RL samples at 0 mM NaCl and their best fits obtained with flexible cylinders (worm-like model within the MSDP approach - see text for details). Curves have been stacked by a factor 10^k, where k is the index of the curves, starting from the one at the bottom with $k = 0$. B) Volume fraction distribution of the chemical groups of di-RL at 0 mM NaCl resulting from the fit of the curve at $C_d = 110$ mM. Red, orange, magenta, blue, dark-green and green lines correspond to CH_2, CH_3, CR, RHA-RHA (Fig. 1), Na^+ and H_2O groups. The curve of Na^+ has been multiplied by a factor 100 for clarity. C) Electron density profile calculated from the volume fraction distributions shown in panel B (black line) together with the contribution of each group (colored lines).

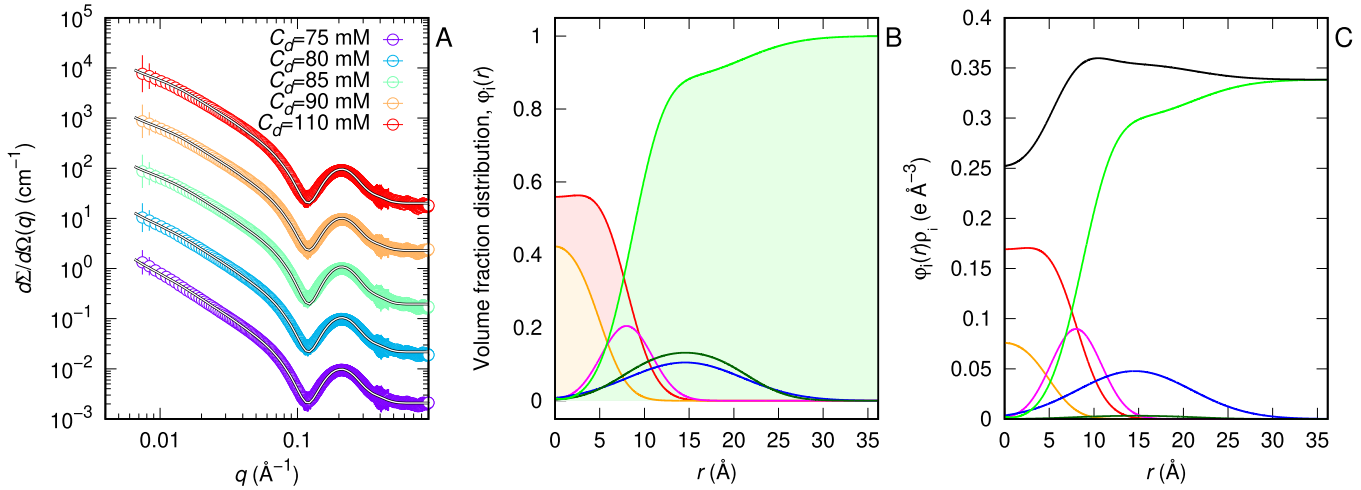

Fig. 5. A) Log-log plot of SAXS curves of di-RL samples at 100 mM NaCl and their best fits obtained with flexible cylinders (worm-like model within the MSDP approach - see text for details). Curves have been stacked by a factor 10^k, where k is the index of the curves, starting from the one at the bottom with $k = 0$. B) Volume fraction distribution of the chemical groups of di-RL at 100 mM NaCl resulting from the fit of the curve at $C_d = 110$ mM. Red, orange, magenta, blue, dark-green and green lines correspond to CH_2, CH_3, CR, RHA-RHA (Fig. 1), Na^+ and H_2O groups. The curve of Na^+ has been multiplied by a factor 100 for clarity. C) Electron density profile calculated from the volume fraction distributions shown in panel B (black line) together with the contribution of each group (colored lines).

density of the water solution (0.33 e/Å^3), the apolar groups exhibit a lower electron density, reaching a minimum of approximately 0.25 e/Å^3 at the axis of the cylinder. Due to the significant presence of water, the electron density of the polar domain reaches a maximum value slightly exceeding 0.35 e/Å^3: in the absence of NaCl (Fig. 4C), the maximum is attained at a radial distance of approximately 10 Å, which decreases to around 8 Å at 110 mM NaCl (Fig. 5C). By looking to the SAXS data, the more marked effect of NaCl is the modification of the curves at low q. The larger differences are seen in either the worm-like chain parameters and in the fractal structure factor parameters. In fact, the Khun length b changes from ≈ 50 to ≈ 90 Å and the number of statistical chain segments from 4 to 13, indicating that the presence of NaCl induces longer worm-like micelles. Moreover, the structure factor parameters are in agreement with this result: the average inhomogeneity radius, r_0 is lower in the presence of NaCl (≈ 190 Å) than in its absence (≈ 330 Å), and the same trend is seen for the correlation length ξ, which decreases from ≈ 2000 Å to ≈ 1400 Å when 100 mM of NaCl is added. The fractal dimension d_f is close to 3 both in the presence and in the absence of NaCl.

To get the di-RL conformations in flexible cylindrical-like micelles, we also applied the MC methodology (Eq. S75) described in Section S5 of SM, combined with SAXS data analysis results (Table S3 of the SM). Fig. 6A and 7A present the 20 most preferred di-RL conformations obtained by MC from the best fittings (Figs. S5 and S6) to the volume fraction distributions of the chemical groups obtained from the SAXS results (Figs. 4B and 5B) from 70 mM di-RL in the absence of NaCl and from 100 mM di-RL at 100 mM NaCl, respectively. The corresponding worm-like micelles formed by these conformers are displayed in Figs. 6B and 7B in the absence and presence of NaCl, respectively.

Interestingly, formation of worm-like micelles by di-RL-C10-C10 was previously predicted by simulation [16], and is now determined by our SAXS analysis.

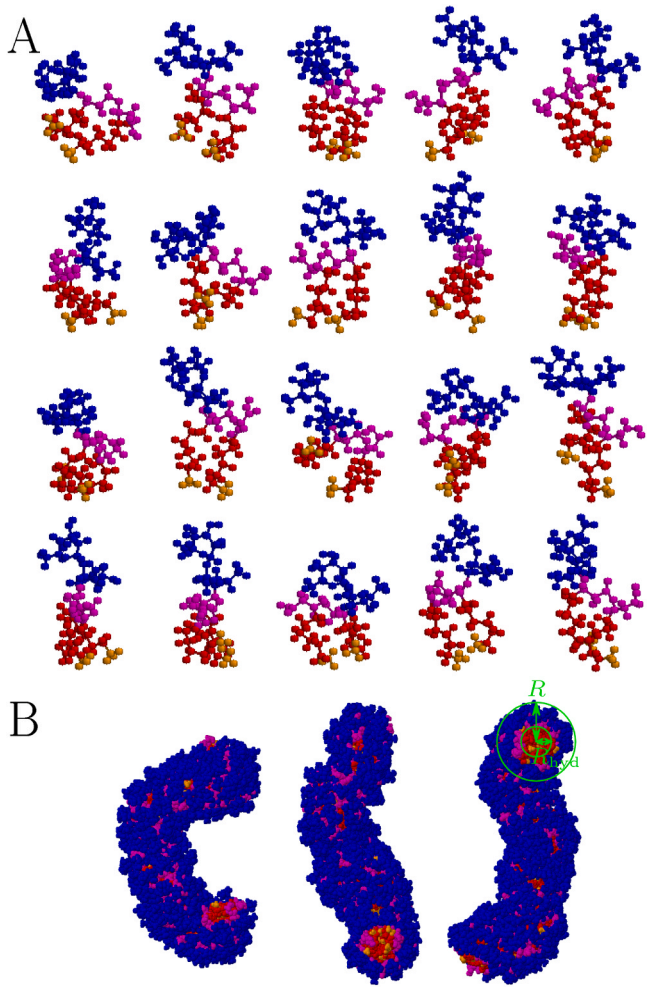

Fig. 6. A) The 20 preferred conformers (Figures S5 and S7) of di-RL obtained by the fit with the Monte Carlo method of the volume fraction distributions derived by the analysis of the SAXS curve with $C_d = 70$ mM and [NaCl]=0 mM. B) Representation of di-RL worm-like micelles obtained by using the best 20 conformers shown in panel A organized according to the best fit parameters of the SAXS curve. According to the definition of Khun length, the represented Kratky-Porod chains have been obtained by using n_l segments of length l_0 with $l_0 = b(1-\cos\theta)/(1+\cos\theta)$ and $n_l = n_b(1+\cos\theta)/(1-\cos\theta)$, where the bond angle θ was fixed at 45°. Horizontal and vertical green double arrows indicate the radius of the hydrated monolayer cylinder, R, and the hydrophobic radius, R_{hyd}, respectively.

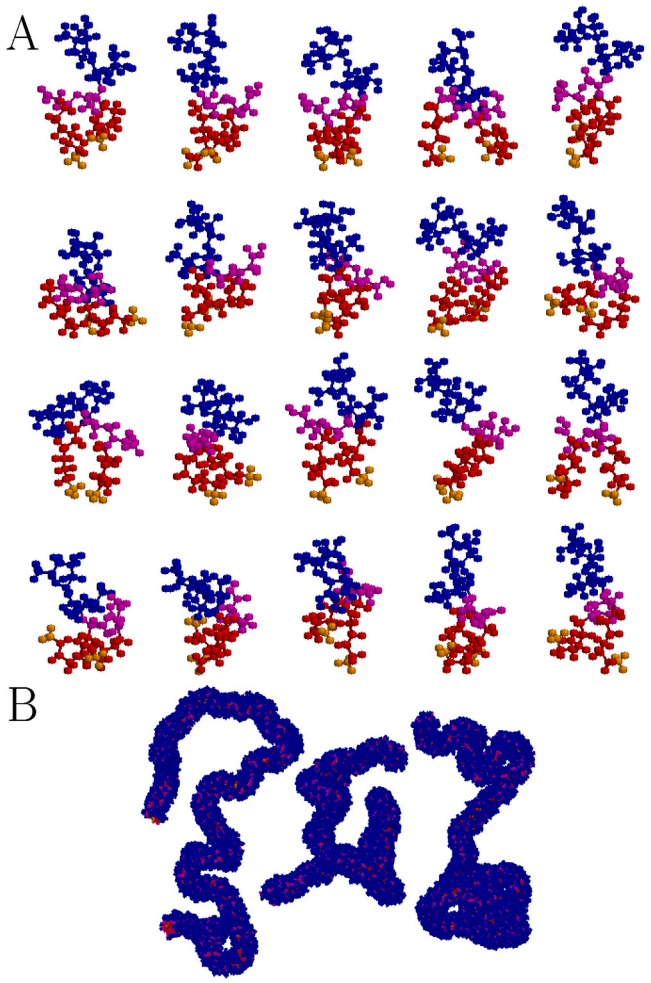

Fig. 7. A) The 20 preferred conformers (Figure S6 and S8) of di-RL obtained by the fit with the Monte Carlo method of the volume fraction distributions derived by the analysis of the SAXS curve with $C_d = 110$ mM and [NaCl]= 100 mM. B) Representation of di-RL worm-like micelles obtained by using the best 20 conformers shown in panel A organized according to the best fit parameters of the SAXS curve. According to the definition of Khun length, the represented Kratky-Porod chains have been obtained by using n_l segments of length l_0 with $l_0 = b(1-\cos\theta)/(1+\cos\theta)$ and $n_l = n_b(1+\cos\theta)/(1-\cos\theta)$, where the bond angle θ was fixed at 45°.

4. Concluding remarks

Rhamnolipids are a kind of glycolipid biosurfactant produced by *Pseudomonas aeruginosa* and other bacterial species. The variety of RLs' chemical structures [5] features their wide range of applications [1,39,40]. In spite of their importance, many RLs self-assembled morphologies have been reported in the literature from globular, cylinder-like micelles and small and large vesicles/lamellar structures depending on pH value, mono-RL and di-RL molar ratio, fatty acid chains size, and the presence of additives and co-surfactants [3,11,13,14]. Here, we carefully separated mono-RL-C10-C10 from di-RL-C10-C10 at pH 7.5 (Fig. 1) to shed light onto self-aggregation properties of each molecule in aqueous solution. To do so, SAXS experiments were carried out in the absence and presence of 100 mM NaCl and increasing concentrations of mono-RL and di-RL. SAXS data analysis made use of MSDP methodology coupled to a MC method, where the best volume distribution of the chemical groups within a micelle-like aggregate was determined. Such an approach helped us verifying that mono-RLs prefer to assemble into planar bilayers independent of C_m (from 10 mM to 50 mM) whereas di-RLs associate into flexible cylinders (from 70 to 110 mM). More specifically, we show that mono-RLs form bilayers that are 29.2 Å-thick, with hydrophobic domain of $2D_{hyd}$ of 11.6 Å (Fig. 4). In this way, the two polar groups, CR and RHA, occupy a layer of circa 9 Å in each monolayer. Considering the whole polar space including hydration water (Fig. 2B), the bilayer thickness expands to 41 Å (2*D*, Table S2 of the SM), resulting in 25 water molecules per polar head and 40 % of Na^+ counter ions. Taking into account that the hydrophobic region is thinner than that considered for 7 carbon atoms-long and the wide volume fraction distribution occupied by the tails (Fig. 2B), we suggest that the hydrophobic chains are rather disordered to cover an area per glycolipid of circa 76 $Å^2$. Interestingly, the data also indicated that 30 % of the bilayers are closely stacked ($c = 33.1 \pm 0.3$ Å, Table S2 of the SM) with a small number of correlated bilayers (~ 5). On the other hand, di-RLs in the absence and presence of salt self-assemble into worm-like micelles. The hydrophobic region is similar in both cases (R_{hyd} on the order of 7.5 Å, Table. S3 of the SM) but it is larger than that found for mono-RL (R_{hyd} = 5.8 Å, Table S2 of the SM) as well as the hydrophobic-polar interface of 110 $Å^2$ (Table S3 of the SM). This suggests that the hydrophobic tails

of di-RLs may be less disordered into the cylindrical geometry in comparison to those of mono-RLs in planar bilayer geometry. Interestingly, the radius of the cylinder including the hydration water is larger in the presence of 100 mM NaCl ($R = 36$ Å) than for salt-free di-RL micelles ($R \sim 29$ Å, Table S3 of the SM). In this way, the polar region, the CR and RHA-RHA groups, occupies a 21.5 Å and 28.5 Å thick-layer including 183 and 290 water molecules per polar head in the absence and presence of salt, respectively. In the presence of NaCl, all Na^+ counterions are placed in the polar head region (Fig. 3B). Further, the addition of 100 mM NaCl leads to the formation of longer flexible cylinders (Fig. 6B) in respect to di-RLs in salt-free aqueous solution (Fig. 6B), but does not change their morphology. In the future, we plan to expand the number of experimental conditions to be investigated, also including pH variations, the type of buffer, and the presence of different monovalent and divalent salts. Furthermore, to consolidate the validity of the MSDP methodology here employed, we plan to combine SAXS data with small-angle neutron scattering (SANS) measurements in the future work, in the presence of different mixtures of light water and heavy water. In this way, it will be possible to modify the scattering length density contrast of the different chemical groups and therefore fully exploit the advantages of the MSPD method through a simultaneous analysis of the SAXS and SANS data measured on the same samples. In conclusion, the ability of mono-RL-C10-C10 and di-RL-C10-C10 molecules to differ their self-assembling features in aqueous solution, as well as their interfacial properties, favors the use of these biosurfactants for novel specific applications.

CRediT authorship contribution statement

Alessandra Marega Motta: Writing – original draft, Investigation. **Paolo Mariani:** Investigation. **Rosangela Itri:** Writing – review & editing, Funding acquisition, Conceptualization. **Francesco Spinozzi:** Writing – review & editing, Software, Methodology, Investigation, Formal analysis, Conceptualization.

Declaration of Competing Interest

The authors declare that they have no known competing financial interests or personal relationships that could have appeared to influence the work reported in this paper.

Data availability

Data will be made available on request.

Acknowledgments

This work was partially funded by the European Union - Next Generation EU, Project Code: ECS00000041, Project Title: Innovation, digitalization and sustainability for the diffused economy in Central Italy - VITALITY. RI is recipient from National Council for Scientific and Technological Development (CNPq, Brazil) for research fellowship. The authors would like to thank Diamond Light Source for beamtime (proposal SM28026–1) and the staff of beamlines I22 for assistance with data collection.

Appendix A. Supporting information

Supplementary data associated with this article can be found in the online version at doi:10.1016/j.colsurfb.2024.114038.

References

[1] D. Kitamoto, T. Morita, T. Fukuoka, M. aki Konishi, T. Imura, Self-assembling properties of glycolipid biosurfactants and their potential applications, Curr. Opin. Colloid Interface Sci. 14 (2009) 315–328.
[2] B. Shao, Z. Liu, H. Zhong, G. Zeng, G. Liu, M. Yu, Y. Liu, X. Yang, Z. Li, Z. Fang, J. Zhang, C. Zhao, Effects of rhamnolipids on microorganism characteristics and applications in composting: a review, Microbiol. Res. 200 (2017) 33–44.
[3] R. Esposito, I. Speciale, C. De Castro, G. D'Errico, I. Russo Krauss, Rhamnolipid self-aggregation in aqueous media: A long journey toward the definition of structure-property relationships, Int. J. Mol. Sci. 24 (2023).
[4] F.G. Jarvis, M.J. Johnson, A glyco-lipide produced by pseudomonas aeruginosa, J. Am. Chem. Soc. 71 (1949) 4124–4126.
[5] A.M. Abdel-Mawgoud, F. Lépine, E. Déziel, Rhamnolipids: diversity of structures, microbial origins and roles, Appl. Microbiol. Biotechnol. 86 (2010) 1323–1336.
[6] F.J. Aranda, J.A. Teruel, A. Ortiz, Recent advances on the interaction of glycolipid and lipopeptide biosurfactants with model and biological membranes, Curr. Opin. Colloid Interface Sci. 68 (2023) 101748.
[7] A. Ortiz, J.A. Teruel, M.J. Espuny, A. Marqués, A. Manresa, F.J. Aranda, Effects of dirhamnolipid on the structural properties of phosphatidylcholine membranes, Int. J. Pharm. 325 (2006) 99–107.
[8] E. Haba, A. Pinazo, R. Pons, L. Pérez, A. Manresa, Complex rhamnolipid mixture characterization and its influence on dppc bilayer organization, Biochim. Et. Biophys. Acta (BBA) - Biomembr. 1838 (2014) 776–783.
[9] A. Marega Motta, M. Donato, G. Mobbili, P. Mariani, R. Itri, F. Spinozzi, Unveiling the mono-rhamnolipid and di-rhamnolipid mechanisms of action upon plasma membrane models, J. Colloid Interface Sci. 624 (2022) 579–592.
[10] H. Abbasi, K.A. Noghabi, M.M. Hamedi, H.S. Zahiri, A.A. Moosavi-Movahedi, M. Amanlou, J.A. Teruel, A. Ortiz, Physicochemical characterization of a monorhamnolipid secreted by Pseudomonas aeruginosa MA01 in aqueous media, Exp. Mol. Dyn. Study, Colloids Surf. B, Biointerfaces 101 (2013) 256–265.
[11] B. Dahrazma, C.N. Mulligan, M.-P. Nieh, Effects of additives on the structure of rhamnolipid (biosurfactant): a small-angle neutron scattering (sans) study, J. Colloid Interface Sci. 319 (2008) 590–593.
[12] M.L. Chen, J. Penfold, R.K. Thomas, T.J.P. Smyth, A. Perfumo, R. Marchant, I. M. Banat, P. Stevenson, A. Parry, I. Tucker, I. Grillo, Solution self-assembly and adsorption at the air-water interface of the monorhamnose and dirhamnose rhamnolipids and their mixtures, Langmuir 26 (2010) 18281–18292.
[13] Y. Guo, C.N. Mulligan, M.-P. Nieh, An unusual morphological transformation of rhamnolipid aggregates induced by concentration and addition of styrene: a small angle neutron scattering (sans) study, Colloids Surf. A: Physicochem. Eng. Asp. 373 (2011) 42–50.
[14] J. Liley, J. Penfold, R. Thomas, I. Tucker, J. Petkov, P. Stevenson, I. Banat, R. Marchant, M. Rudden, A. Terry, I. Grillo, Self-assembly in dilute mixtures of non-ionic and anionic surfactants and rhamnolipd biosurfactants, J. Colloid Interface Sci. 487 (2017) 493–503.
[15] B. İkizler, G. Arslan, E. Kipcak, C. Dirik, D. Çelenk, T. Aktuğlu, Ş.Ş. Helvacı, S. Peker, Surface adsorption and spontaneous aggregation of rhamnolipid mixtures in aqueous solutions, Colloids Surf. A: Physicochem. Eng. Asp. 519 (2017) 125–136.
[16] M.-T. Lee, Micellization of rhamnolipid biosurfactants and their applications in oil recovery: insights from mesoscale simulations, J. Phys. Chem. B 125 (2021) 9895–9909.
[17] N. Baccile, A. Poirier, J. Perez, P. Pernot, D. Hermida-Merino, P. LeGriel, C. C. Blesken, C. Müller, L.M. Blank, T. Tiso, Self-assembly of rhamnolipid bioamphiphiles: Understanding the structure-property relationship using small-angle x-ray scattering, Langmuir 39 (2023) 9273–9289.
[18] M. Sánchez, F.J. Aranda, M.J. Espuny, A. Marqués, J.A. Teruel, A. Manresa, A. Ortiz, Aggregation behaviour of a dirhamnolipid biosurfactant secreted by pseudomonas aeruginosa in aqueous media, J. Colloid Interface Sci. 307 (2007) 246–253.
[19] A.J. Smith, S.G. Alcock, L.S. Davidson, J.H. Emmins, J.C. Hiller Bardsley, P. Holloway, M. Malfois, A.R. Marshall, C.L. Pizzey, S.E. Rogers, O. Shebanova, T. Snow, J.P. Sutter, E.P. Williams, N.J. Terrill, I22: SAXS/WAXS beamline at diamond Light Source – an overview of 10 years operation, J. Synchrotron Radiat. 28 (2021) 939–947.
[20] T. Williams, C. Kelley, many others, Gnuplot 4.6: an interactive plotting program, ⟨http://gnuplot.sourceforge.net/⟩ (2013).
[21] F. Spinozzi, C. Ferrero, M.G. Ortore, A.D.M. Antolinos, P. Mariani, GENFIT: software for the analysis of small-angle X-ray and neutron scattering data of macromolecules in-solution, J. Appl. Cryst. 47 (2014) 1132–1139.
[22] R. De Rosa, F. Spinozzi, R. Itri, Hydroperoxide and carboxyl groups preferential location in oxidized biomembranes experimentally determined by small angle x-ray scattering: Implications in membrane structure, BBA - Biomembr. 1860 (2018) 2299–2307.
[23] J.S. Yoneda, D.R. de Araujo, F. Sella, G.R. Liguori, T.T. Liguori, L.F.P. Moreira, F. Spinozzi, P. Mariani, R. Itri, Self-assembled guanosine-hydrogels for drug-delivery application: structural and mechanical characterization, methylene blue loading and controlled release, Mater. Sci. Eng. C. 121 (2021) 111834.
[24] R. Hosemann, S.N. Bagchi, The interference theory of ideal paracrystals, Acta Cryst. 5 (1952) 612–614.
[25] R. Hosemann, S. Bagchi, Direct Analysis of Diffraction by Matter, North-Holland, Amsterdam, 1962.
[26] R. Hosemann, K.L.W. Wilke, The Paracrystal as a Model for Liquid Crystals, Mol. Cryst. 2 (1967) 333–362.
[27] W. Wilke, General lattice factor of the ideal paracrystal, Acta Cryst. A 39 (6) (1983) 864–867.
[28] H. Matsuoka, H. Tanaka, T. Hashimoto, N. Ise, Elastic scattering from cubic lattice systems with paracrystalline distortion, Phys. Rev. B 36 (3) (1987) 1754–1765.
[29] R. Lazzari, Isgisaxs: a program for grazing incidence small-angle x-ray scattering analysis of supported islands, J. Appl. Cryst. 35 (2002) 406.

[30] T. Frühwirth, G. Fritz, N. Freiberger, O. Glatter, Structure and order in lamellar phases determined by small-angle scattering, J. Appl. Cryst. 37 (2004) 703–710.
[31] J.S. Pedersen, P. Schurtenberger, Scattering functions of semiflexible polymers with and without excluded volume effects, Macromolecules 29 (1996) 7602–7612.
[32] O. Glatter, Fourier transformation and deconvolution, in: P. Lindner, T. Zemb (Eds.), Neutron, X-rays and Light. Scattering Methods Applied to Soft Condensed Matter, North-Holland, 2002, pp. 103–124.
[33] F. Spinozzi, L. Paccamiccio, P. Mariani, L.Q. Amaral, Melting REgime of the Anionic Phospholipid DMPG: new lamellar phase and porous bilayer model, Langmuir 26 (2010) 6484–6493.
[34] F. Spinozzi, M.G. Ortore, G. Nava, F. Bomboi, F. Carducci, H. Amenitsch, T. Bellini, F. Sciortino, P. Mariani, Gelling without structuring: a saxs study of the interactions among dna nanostars, Langmuir 36 (2020) 10387–10396.
[35] P. Platform, version 2022.1.2, advanced chemistry development, inc. (acd/labs), toronto, on, canada 2022.(www.acdlabs.com).
[36] J. Nagle, M. Wiener, Structure of fully hydrated bilayer dispersions, Biochim. Et. Biophys. Acta (BBA) - Biomembr. 942 (1988) 1–10.
[37] P. Balgavý, M. Dubničková, N. Kučerka, M.A. Kiselev, S.P. Yaradaikin, D. Uhríková, Bilayer thickness and lipid interface area in unilamellar extruded 1,2-diacylphosphatidylcholine liposomes: a small-angle neutron scattering study, Biochim. Et. Biophys. Acta (BBA) - Biomembr. 1512 (2001) 40–52.
[38] S.J. Marrink, A.H. de Vries, A.E. Mark, Coarse grained model for semiquantitative lipid simulations, J. Phys. Chem. B 108 (2004) 750–760.
[39] J. Chen, Q. Wu, Y. Hua, J. Chen, H. Zhang, H. Wang, Potential applications of biosurfactant rhamnolipids in agriculture and biomedicine, Appl. Microbiol. Biotechnol. 101 (2017) 8309–8319.
[40] P. Thakur, N.K. Saini, V.K. Thakur, V.K. Gupta, R.V. Saini, A.K. Saini, Rhamnolipid the glycolipid biosurfactant: Emerging trends and promising strategies in the field of biotechnology and biomedicine, Microb. Cell Factor. 20 (2021) 1.